Volume 8
Number 5
7 February 2020
Pages 1479–1888

Journal of Materials Chemistry C

Materials for optical, magnetic and electronic devices

rsc.li/materials-c

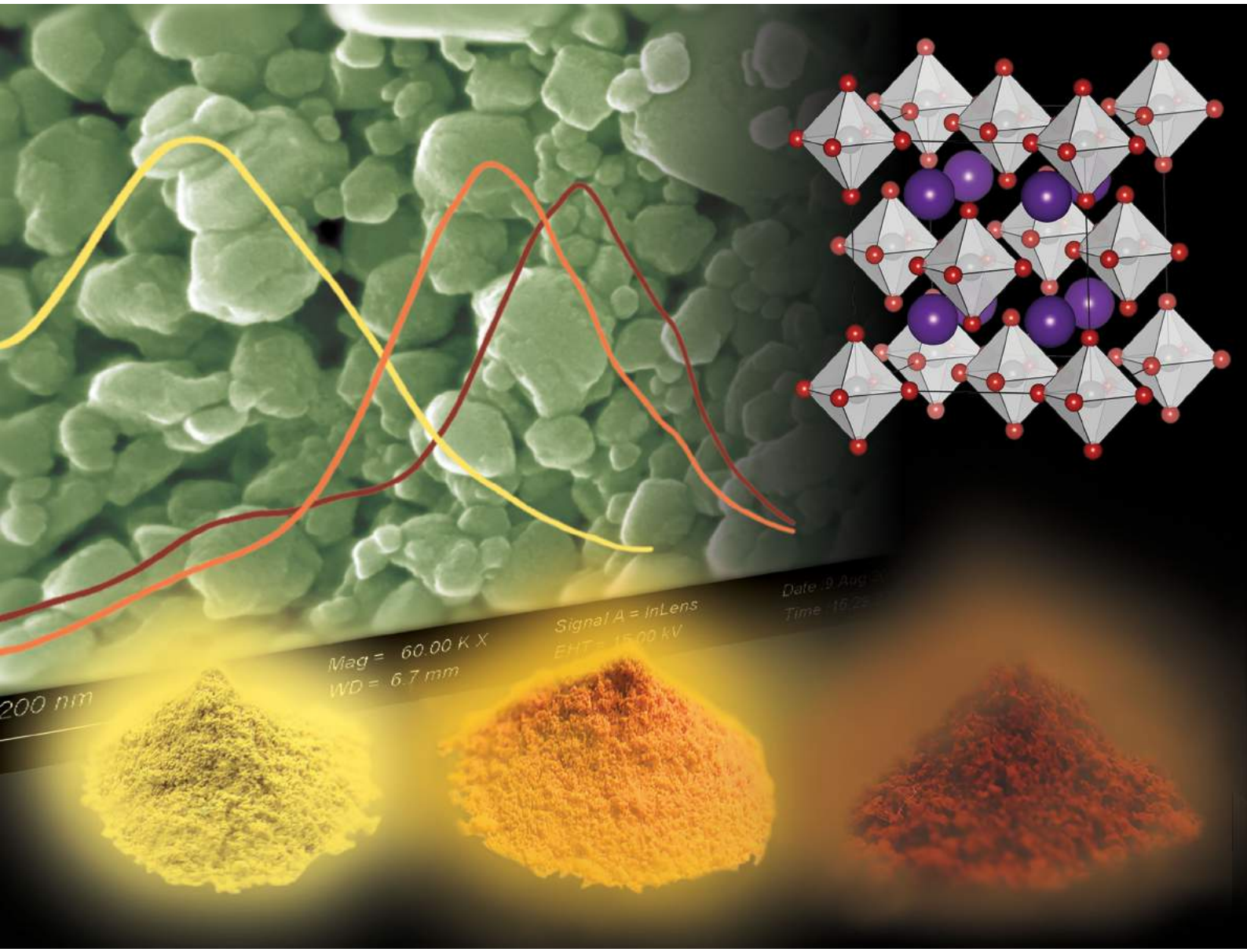

ISSN 2050-7526

ROYAL SOCIETY OF CHEMISTRY

PAPER

Xing Sheng, Lan Yin *et al.*

Solution processed lead-free cesium titanium halide perovskites and their structural, thermal and optical characteristics

Journal of Materials Chemistry C

ROYAL SOCIETY OF CHEMISTRY

PAPER

View Article Online
View Journal | View Issue

Cite this: J. Mater. Chem. C, 2020, 8, 1591

Solution processed lead-free cesium titanium halide perovskites and their structural, thermal and optical characteristics

Deying Kong,†[a] Dali Cheng,†[b] Xuewen Wang,[a] Kaiyuan Zhang,[b] Huachun Wang,[b] Kai Liu,[a] Huanglong Li,[c] Xing Sheng*[b] and Lan Yin*[a]

Received 18th October 2019,
Accepted 3rd December 2019

DOI: 10.1039/c9tc05711k

rsc.li/materials-c

Metal halide based perovskite materials have attracted tremendous interest in optoelectronics. Although conventional lead (Pb) based organic/inorganic halide perovskites have been extensively studied and have realized highly efficient devices like solar cells and light emitting diodes, they are plagued with the toxicity of the Pb element, restraining their applications in environmentally and biologically friendly scenarios. Substitutes for Pb ions have been suggested, yet most of the Pb-free perovskites suffer from low stability and inferior efficiencies compared to their Pb based counterparts. In this work, we explore the synthesis of cesium titanium halide perovskites (Cs_2TiX_6, X = Cl, Br). At room-temperature, aqueous solution-based processes are developed to grow thermally stable, high quality $Cs_2Ti(Br_xCl_{1-x})_6$ ($0 < x < 1$) crystals and films in large volume. Their structural, thermal and optical properties are systematically studied in experiments and compared with first principles calculations. The produced materials demonstrate a tunable, quasi-direct band gap from ~1.7 eV to ~2.5 eV and photoluminescence peaked from ~535 nm to ~670 nm. Furthermore, the materials are stable in an ambient environment up to ~500 °C. These Pb-free perovskite materials will create opportunities for novel optical and electronic devices used in eco-friendly and bio-friendly environments.

1. Introduction

The past decade has witnessed a significant surge of research on metal halide based perovskite materials for optoelectronic applications, because of their excellent electron-photon conversion efficiency, ease of fabrication, and outstanding tolerance of defects.[1] Recent advances have led to high performance optoelectronic devices, with remarkable examples including perovskite-based light-emitting diodes (LEDs) with external quantum efficiencies exceeding 20%[2] and photovoltaic (PV) cells with one-sun efficiencies of over 20%.[3] In particular, most of these high performance devices are based on lead (Pb) halide perovskites, which are endowed with high optical absorption and emission efficiencies associated with their direct band gaps.[4] However, the toxicity of Pb hinders their use in environmental and biomedical applications, and Pb-free materials and devices are highly demanded.[5] To bypass this challenge, attempts have been made by employing different inorganic metal cations to substitute Pb^{2+} in halide perovskite systems, including tellurium (Te^{4+}),[6] germanium (Ge^{4+}),[7] tin (Sn^{2+}),[8] copper (Cu^{2+}),[9] bismuth (Bi^{3+}),[10] antimony (Sb^{3+})[11] and silver (Ag^{+}).[12] Unfortunately, devices based on these materials suffer from poor optoelectronic efficiencies and low stability in ambient environments. Moreover, most of these substitute ions are still not compatible with eco-friendly and bio-friendly environments.

More recently, titanium (Ti) based halide perovskites have been proposed as an alternative and promising solution to Pb-free perovskites for optoelectronic devices, and preliminary experiments have demonstrated cesium titanium bromide (Cs_2TiBr_6) based solar cells with a power conversion efficiency (PCE) of about 3%.[13,14] Attributed to the desirable biocompatibility and eco-friendliness of Ti, such materials are considered to be an ideal candidate for Pb-free halide perovskites. The synthesis of Cs_2TiBr_6 presented in previous reports, however, involves vacuum based evaporation and annealing at elevated temperatures (>200 °C) in a $TiBr_4$-vapor atmosphere, which are unfavorable for low-cost fabrication at large scale. Furthermore, Ti based halide perovskites with band gaps larger than Cs_2TiBr_6

[a] School of Materials Science and Engineering, The Key Laboratory of Advanced Materials of Ministry of Education, State Key Laboratory of New Ceramics and Fine Processing, Tsinghua University, Beijing, 100084, China. E-mail: lanyin@tsinghua.edu.cn
[b] Department of Electronic Engineering, Beijing National Research Center for Information Science and Technology, Tsinghua University, Beijing, 100084, China. E-mail: xingsheng@tsinghua.edu.cn
[c] Department of Precision Instrument, Tsinghua University, Beijing, 100084, China
† D. K. and D. C. contributed equally to this work.

and optical emissions in the visible range have not been realized.

In this work, we demonstrate the synthesis of a family of cesium titanium bromide chloride perovskites, $Cs_2Ti(Br_xCl_{1-x})_6$ ($0 < x < 1$), through a full aqueous solution process at room temperature. Cs_2TiCl_6, Cs_2TiBr_6 and $Cs_2TiBr_2Cl_4$ crystals and films are formed, and their structural, thermal and optical properties are systematically characterized and compared with first-principles calculations. We find that these materials have quasi-direct band gaps. By adjusting the molar ratio of Cl and Br, the $Cs_2Ti(Br_xCl_{1-x})_6$ materials exhibit tunable band gaps from ~1.7 eV (for Cs_2TiBr_6) to ~2.5 eV (for Cs_2TiCl_6) and photoluminescence emission peaking from ~535 nm (for Cs_2TiCl_6) to ~670 nm (for Cs_2TiBr_6). Moreover, these materials present high thermal stabilities, with decomposition temperatures above 500 °C. By studying these materials, we hope to provide viable pathways to next-generation Pb-free high-performance optoelectronic materials and devices for eco-friendly and bio-friendly applications.

2. First-principles calculations

Fig. 1a schematically illustrates the crystal structure of Cs_2TiX_6 (X = Cl, Br, or I), which has a vacancy-ordered halide double perovskite lattice. Herein, we focus on the study of $Cs_2Ti(Br_xCl_{1-x})_6$ ($0 < x < 1$), since it has a tunable optical band gap in the visible spectral range. The band gap is calculated by performing first-principles density functional theory (DFT) simulations, and is plotted in Fig. 1b. By adjusting the ratio between the two halogens, Br and Cl (x = 0, 1/6, 1/3, 1/2, 2/3, 5/6, and 1), the calculated electronic band gap exhibits a tunability from ~1.6 eV (for Cs_2TiBr_6) to ~2.3 eV (for Cs_2TiCl_6). It should be noted that for the cases where x = 1/3, 1/2 and 2/3, various geometric arrangements of different halogen atoms (Br and Cl) in a $[TiX_6]^{2-}$ octahedron exist, rendering the different calculated band gaps observed in Fig. 1b. We can also observe that the band gap variance does not follow a perfect linear relation with x, which can be explained by possible lattice distortions and differences of arrangement orders in $Cs_2Ti(Br_xCl_{1-x})_6$.[14] Fig. 1c and d plot calculated electronic band diagrams for Cs_2TiBr_6 and Cs_2TiCl_6, respectively. While both Cs_2TiBr_6 and Cs_2TiCl_6 exhibit indirect band gaps, their band valleys at the Γ and X points are very close, with differences of <100 meV. Therefore, their band structures can be referred to as quasi-direct. More detailed analysis reveals that the valence band maximum (VBM) located at the Γ point is primarily contributed by p states of halogen atoms, while the conduction band minimum (CBM) at the X point is contributed by d states of Ti.

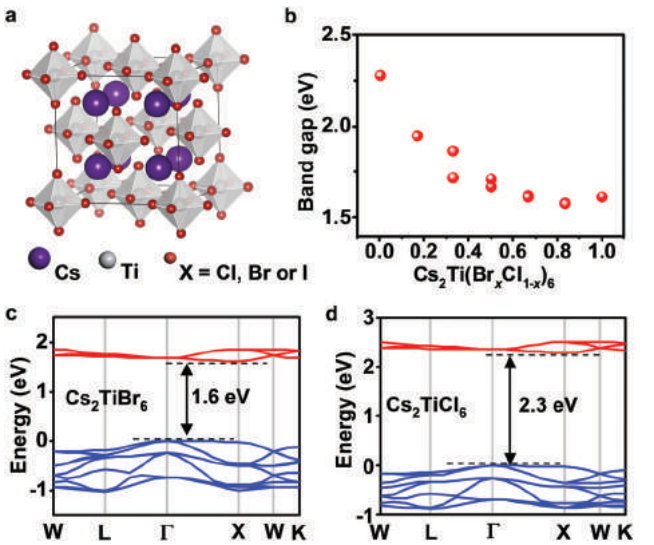

Fig. 1 (a) Crystal structure of Cs_2TiX_6 (X = Cl, Br or I). (b) Calculated band gaps of $Cs_2Ti(Br_xCl_{1-x})_6$ ($0 < x < 1$), using density functional theory (DFT) from first principles. The relative positions of the Br and the Cl atoms are adjacent or coplanar when x = 1/3, 1/2 and 2/3. (c and d) Calculated electronic band diagrams of (c) Cs_2TiBr_6 and (d) Cs_2TiCl_6.

3. Structural characterization

To experimentally synthesize the numerically predicted materials in Fig. 1, we develop a solution-based process to produce $Cs_2Ti(Br_xCl_{1-x})_6$ ($0 < x < 1$) under ambient conditions at room temperature. As-prepared Cs_2TiCl_6, Cs_2TiBr_6 and $Cs_2TiBr_2Cl_4$ crystals are shown in Fig. 2a, b and c, respectively. For example, to make Cs_2TiCl_6, a saturated aqueous solution of cesium chloride (CsCl) is mixed with a concentrated hydrochloric acid (HCl) solution. After dropping excessive titanium chloride ($TiCl_4$) liquid into the mixed solution, the clear solution immediately transforms into a yellowish suspension made of crystallized Cs_2TiCl_6 (Fig. 2a):[15]

$$2CsCl + TiCl_4 = Cs_2TiCl_6$$

A similar reaction can be designed to form Cs_2TiBr_6 crystals using cesium bromide (CsBr) and titanium bromide ($TiBr_4$), which presents a dark, brownish color (Fig. 2b):

$$2CsBr + TiBr_4 = Cs_2TiBr_6$$

Finally, $Cs_2Ti(Br_xCl_{1-x})_6$ ($0 < x < 1$) can be formed by mixing CsCl, $TiCl_4$, CsBr and $TiBr_4$. The stoichiometric ratio x can be deduced by the measured lattice constants from X-ray diffraction results, which will be discussed subsequently. Fig. 2c presents the synthesized $Cs_2TiBr_2Cl_4$ crystals with an orange color. All the powders exhibit a polycrystalline structure, with a grain size of 100–200 nanometers. Fig. 2d–i present zoom-in scanning electron microscopy (SEM) images and corresponding energy-dispersive X-ray spectroscopy (EDS) element mappings of Br and Cl for Cs_2TiCl_6, Cs_2TiBr_6 and $Cs_2TiBr_2Cl_4$ samples, respectively. It can be seen that Br and Cl co-exist uniformly in $Cs_2TiBr_2Cl_4$ grains, indicating that the produced perovskite with mixed halogens is a single phase material, instead of a mixture of Cs_2TiCl_6 and Cs_2TiBr_6 grains. Using such a solution process, these materials can be rapidly and massively produced from 0 °C to room temperature, either in a glovebox or in ambient environments, with no significant differences based on

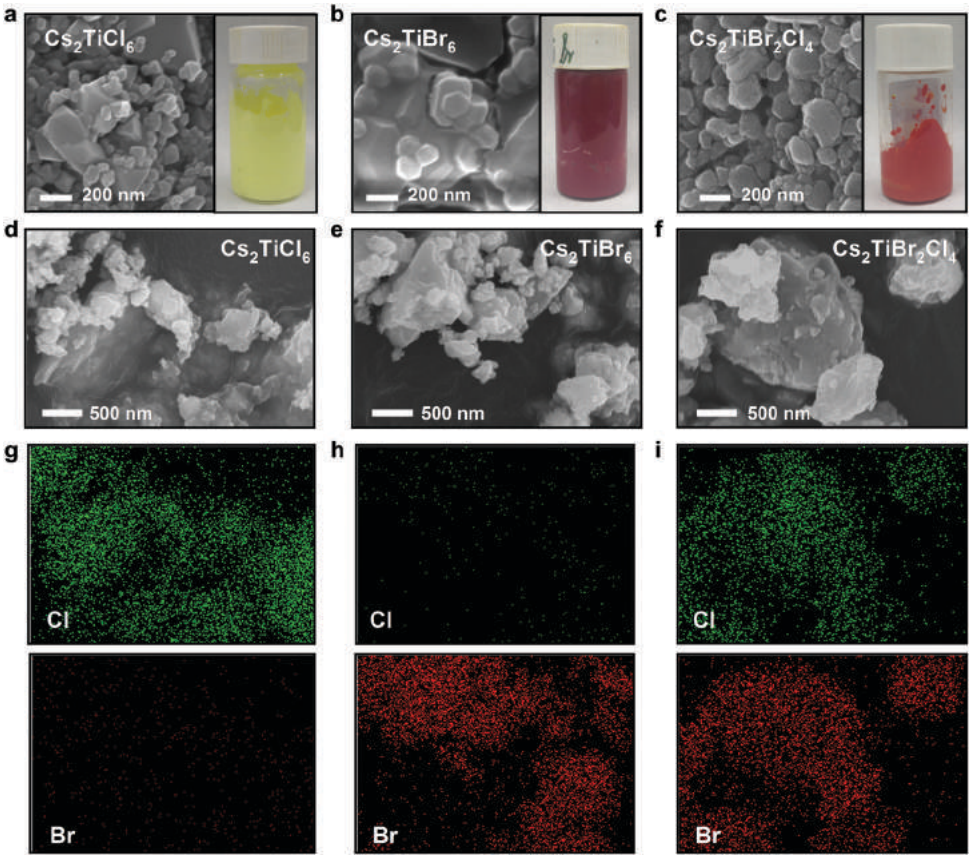

Fig. 2 (a–c) Scanning electron microscopy (SEM) images and corresponding photographs of synthesized (a) Cs_2TiCl_6, (b) Cs_2TiBr_6, and (c) $Cs_2TiBr_2Cl_4$ crystals. (d–i) Zoom-in SEM images and corresponding energy-dispersive X-ray spectroscopy (EDS) element mappings of Br and Cl in (d and g) Cs_2TiCl_6, (e and h) Cs_2TiBr_6, and (f and i) $Cs_2TiBr_2Cl_4$ crystals.

observation and structural characterization. Furthermore, the process eliminates the requirements of vacuum based deposition, high temperature annealing and the inert atmosphere used in previous reports.[13] Based on our current process, the formed crystals exhibit a very porous structure, which is not ideal for realizing thin-film devices. In the future, we will further explore solvents to disperse and dissolve these crystals, and facilitate the formation of denser films for practical applications.

Our solution processed $Cs_2Ti(Br_xCl_{1-x})_6$ based perovskite structures are further confirmed by measured X-ray diffraction (XRD) results plotted in Fig. 3. The diffractive peaks of Cs_2TiCl_6 and Cs_2TiBr_6 are in accordance with those of their respective

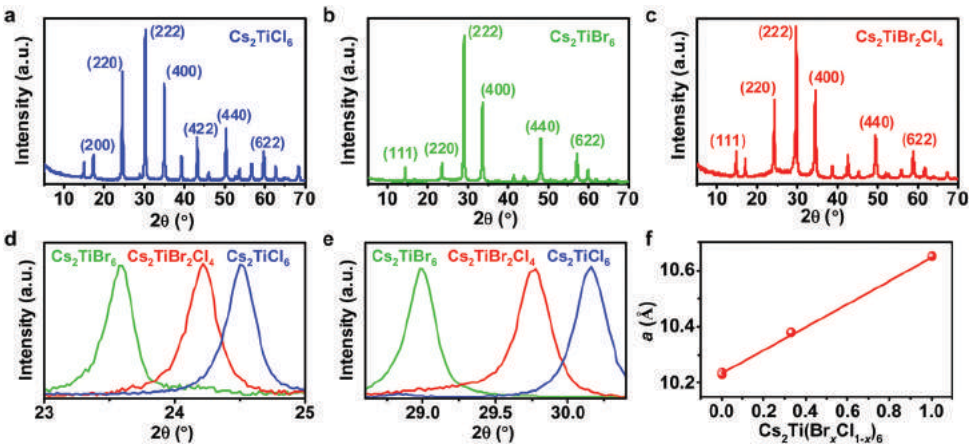

Fig. 3 (a–c) X-ray diffraction (XRD) patterns of (a) Cs_2TiCl_6, (b) Cs_2TiBr_6, and (c) $Cs_2TiBr_2Cl_4$ crystals. (d and e) Diffraction peaks for (d) the (220) and (e) the (222) planes of Cs_2TiCl_6, Cs_2TiBr_6, and $Cs_2TiBr_2Cl_4$ crystals. (f) Calculated lattice constants of $Cs_2Ti(Br_xCl_{1-x})_6$ ($0 < x < 1$) based on XRD results.

materials in the database, which are formed using high temperature sintering methods, as shown in Fig. 3a and b,.[13,16] Results of the $Cs_2TiBr_2Cl_4$ sample (Fig. 3c) present a similar, single-phase perovskite structure. Some unmatched peaks in the XRD patterns correspond to the residues of unreacted CsCl and CsBr in the products. Fig. 3d and e respectively present zoom-in diffractive peaks of crystal planes (220) and (222) for the three different crystals. The results indicate that an increase of Br in the crystals shifts the diffraction peaks to smaller angles, thus resulting in an expanded lattice. Based on these XRD results, the lattice constant a is calculated for the three different perovskites and shown in Fig. 3f. Using Bragg's law, lattice constants for Cs_2TiCl_6 and Cs_2TiBr_6 are determined to be 10.235 Å and 10.652 Å, respectively, in agreement with reported crystals in the database.[15] Based on Vegard's law, we assume that the lattice constant of $Cs_2Ti(Br_xCl_{1-x})_6$ is approximately a weighted mean of Cs_2TiCl_6 and Cs_2TiBr_6, and the produced crystal in our work here with a = 10.381 Å is determined to be $Cs_2TiBr_2Cl_4$ ($x \approx 0.33$).

4. Material stabilities

Another feature worth mentioning for these materials is their structural stability. Fig. 4 evaluates the thermal stabilities of our synthesized perovskite crystals. Fig. 4a–c plot the results of thermogravimetric analysis (TGA) for Cs_2TiCl_6, Cs_2TiBr_6 and $Cs_2TiBr_2Cl_4$ samples, respectively. For all the samples, the minor drop of weight (~10%) below ~200 °C is associated with the evaporation of remaining residues, mostly water and titanium halides ($TiCl_4$ and $TiBr_4$) within the materials. Fig. 4d and e verify that the X-ray diffractive peaks show no obvious changes after heating the as-prepared Cs_2TiCl_6 and Cs_2TiBr_6 crystals at 200 °C for 6 hours. In addition, they remain stable in an ambient atmosphere (20 °C, relative humidity 30%) for 4 hours, except that some small signals of CsBr are observed in Fig. 4e. The next drops in the TGA curves occur above 500 °C, ascribed to the decomposition of perovskites:

$$Cs_2TiX_6 = 2CsX + TiX_4 \ (X = Cl \text{ and } Br)$$

in which cesium halides (CsCl and CsBr) are solids, and titanium halides ($TiCl_4$ and $TiBr_4$) are volatile. Measured weight changes of all three samples using TGA are consistent with the stoichiometric ratios of CsX and TiX_4 in the decomposition reactions. Specifically, the decomposition temperatures are ~520 °C, ~580 °C, and ~560 °C for Cs_2TiCl_6, Cs_2TiBr_6 and $Cs_2TiBr_2Cl_4$ samples, respectively. These decomposition temperatures are much higher than those of organic Pb perovskites (decomposition temperature below ~300 °C)[17] and comparable to those of inorganic Pb and Ag-Bi based perovskites.[17,18] These results suggest that devices based on these Cs_2TiX_6 perovskites can operate at elevated temperatures with high stabilities.

5. Optical properties

To assess the potential of using these perovskite materials in optoelectronic devices, the optical properties of Cs_2TiCl_6, Cs_2TiBr_6 and $Cs_2TiBr_2Cl_4$ films are measured and displayed in Fig. 5. All these materials are cast on quartz substrates, with

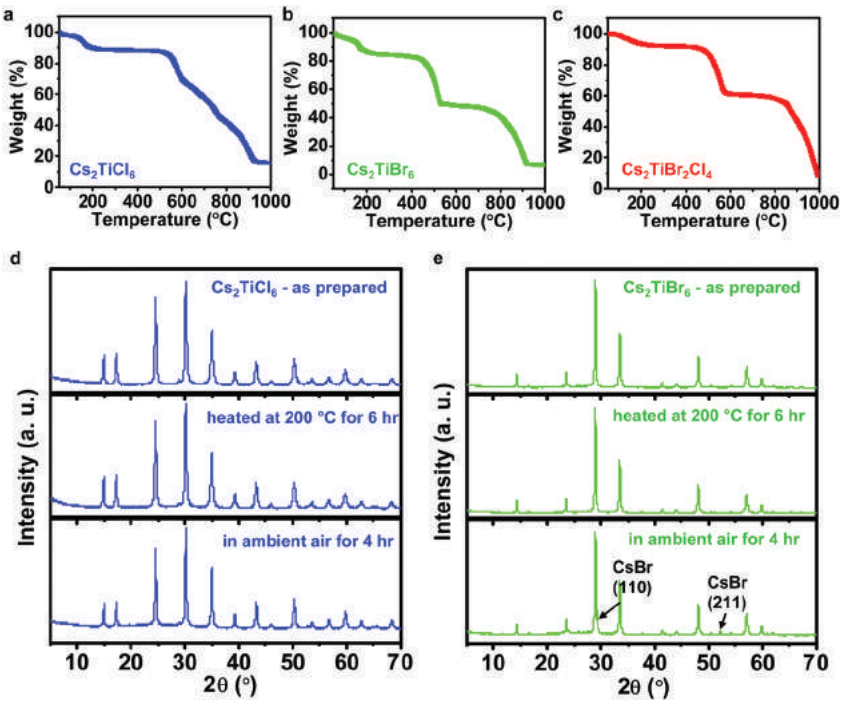

Fig. 4 (a–c) Thermogravimetric analysis (TGA) of (a) Cs_2TiCl_6, (b) Cs_2TiBr_6, and (c) $Cs_2TiBr_2Cl_4$ crystals. (d and e) X-ray diffraction (XRD) patterns of (d) Cs_2TiCl_6 and (e) Cs_2TiBr_6 under different conditions: as prepared, after heating at 200 °C for 6 hours and in ambient air (20 °C, Relative humidity 30%) for 4 hours.

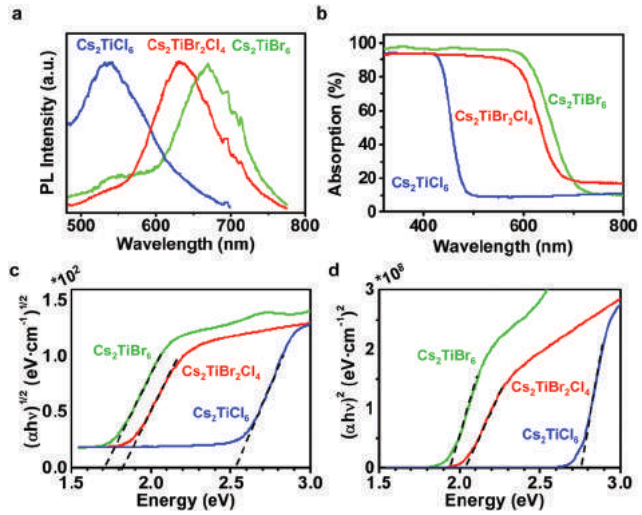

Fig. 5 (a) Photoluminescence (PL) spectra (excited by a 365 nm LED), and (b) absorption spectra of Cs_2TiCl_6, Cs_2TiBr_6, and $Cs_2TiBr_2Cl_4$ films. (c and d) Tauc plots of absorption coefficients *versus* photon energy (c) for indirect allowed transitions and (d) for direct allowed transitions.

a film thickness of approximately 50 μm. With a 365 nm ultraviolet (UV) LED as the excitation source, steady-state photoluminescence (PL) spectra of the perovskite films are acquired and plotted in Fig. 5a. The emission peaks of Cs_2TiCl_6, $Cs_2TiBr_2Cl_4$ and Cs_2TiBr_6 are centered at ~535 nm, ~635 nm and ~670 nm, corresponding to the transition energies of ~2.3 eV, ~1.95 eV and 1.85 eV, respectively. For all the PL peaks, the full width at half maximum (FWHM) values are ~100 nm, larger than the conventional III–V semiconductor emitters and Pb-based halide perovskites. Measured photoluminescence quantum yields (PLQYs) are much less than 1%. These results can be attributed to the indirect nature of the band gaps for these materials. Fig. 5b plots the optical absorption spectra of these perovskite films on quartz substrates. Based on these measured absorption spectra, the absorption coefficient α and photon energy $h\nu$ are calculated, and Tauc plots of $(\alpha h\nu)^{1/2}$ *vs.* $h\nu$ and $(\alpha h\nu)^2$ *vs.* $h\nu$ are presented in Fig. 5c and d, respectively. Band gaps for optical transitions can be deduced from the intercepts of the linear part of the Tauc curves. Indirect band gaps of the materials can be estimated to be ~2.54 eV (Cs_2TiCl_6), ~1.82 eV ($Cs_2TiBr_2Cl_4$) and ~1.7 eV (Cs_2TiBr_6) (Fig. 5c), while direct band gaps are ~2.75 eV (Cs_2TiCl_6), ~2.03 eV ($Cs_2TiBr_2Cl_4$) and ~1.94 eV (Cs_2TiBr_6) (Fig. 5d). It is noted that the PL emission peak of Cs_2TiCl_6 is more red-shifted compared to those of $Cs_2TiBr_2Cl_4$ and Cs_2TiBr_6, which is probably also attributed to the nature of the indirect band gaps of the materials. Similar behaviors have also been observed in other lead-free perovskites like $Cs_2AgBiBr_6$.[19] The results are in accordance with numerical predictions in Fig. 1, with remaining discrepancies that can be explained by the limitations of the general-gradient-approximation (GGA) functional used here. In such a model, standard DFT exchange–correlation functions, including local density approximation (LDA) and GGA, tend to underestimate the band gaps of semiconductor materials because of the derivative discontinuity of energy with respect to the number of electrons in the system.[20] Moreover, DFT calculation results represent the atomic and electronic structures of Cs_2TiX_6 crystals at 0 K, thus also contributing to the remaining deviation considering that the experiments are performed at room temperature.

6. Conclusion

To summarize, we demonstrate that the titanium-based halide perovskites $Cs_2Ti(Br_xCl_{1-x})_6$, with a tunable band gap and optical absorption in the visible range, can be synthesized rapidly at a large scale, using an aqueous solution based process at room temperature, with the produced materials exhibiting excellent thermal stabilities. Although these preliminary results indicate that these as-prepared Cs_2TiX_6 perovskites do not possess optimal properties for photon emission due to their indirect band gap, further routes can be explored to engineer their band structures. Since the direct and indirect band gaps are so close in these materials, strategies like strain engineering and chemical doping can possibly be applied to alter the electronic bands towards direct band gap semiconductors.[21] In addition, developing processes to form nanocrystals and quantum dots,[22] alloying with other metallic or halide elements,[23,24] defect engineering and surface passivation[25] could also improve the materials' photo emission efficiencies. Although the materials possess high thermal stabilities, they easily decompose in high-moisture environments, similar to other halides. Therefore, explorations including optimizing the surface passivation and/or adding waterproof protection deserve further investigation. Furthermore, to fabricate thin-film devices, high-quality films with controlled crystallinity and thicknesses could be realized using methods like spin coating and post annealing in a modified solution.[26] Performance improvements can also be achieved by combining these perovskites with other materials to form heterogeneous junctions and device structures. Besides photo emission and detection, other applications like electrochromic and photochemical sensing[27] can also be exploited. Similar to Ti, other Group IVb elements like zirconium (Zr) and hafnium (Hf) could also form lead-free halide perovskites and their scintillating properties have been preliminarily studied.[28] The results discussed here provide evidence of the low-cost, solution-processed Pb-free Cs_2TiX_6 perovskites as promising candidates of next generation eco-friendly and bio-friendly optoelectronic materials and devices.

Experimental section

Materials and synthesis

Cesium bromide (CsBr, 99.999%) was purchased from Sigma Aldrich. Cesium chloride (CsCl, 99.9%) was purchased from Innochem. Titanium bromide ($TiBr_4$, 98%) and titanium chloride ($TiCl_4$, 99%) were purchased from Alfa Aesar. Hydrobromide acid solution (HBr, 48%) was purchased from Aladdin. Hydrochloride acid solution (HCl, 36%) was purchased from Tongguang Beijing. Chlorobenzene (CB, 99.8%) was purchased from Acros.

Cs_2TiBr_6 was synthesized by adding $TiBr_4$ into aqueous hydrobromic acid solution with saturated CsBr (1 g ml^{-1}) (molar ratio of $TiBr_4$ and CsBr is 1.3 : 1). Cs_2TiCl_6 perovskites were synthesized with a similar method by replacing all bromide with chloride. To form the bromochloride titanium perovskite $Cs_2Ti(Br_xCl_{1-x})_6$, CsBr and CsCl were dissolved in aqueous hydrobromic and hydrochloric acid solution (total 1 g ml^{-1}) with the Br and Cl molar ratio of $x:(1-x)$, and $TiBr_4$ and $TiCl_4$ were dissolved with an equivalent ratio in chlorobenzene ($\sim$total 1 g ml^{-1}); the molar ratio of titanium halides with titanium cesium is 1.3 : 1. An orangish perovskite suspension occurred immediately when mixing the two precursors. After the reaction, chlorobenzene floated above the produced perovskite suspension and was removed.

The as-prepared perovskite suspension was then cast onto quartz substrates in an argon-filled glovebox to volatilize redundant water and titanium halides overnight at room temperature. Powder samples for subsequent characterization were obtained by scratching the materials off the substrate and grinding them in a mortar.

Material characterization

Scanning electron microscopy (SEM) and energy-dispersive X-ray spectroscopy (EDS) images were collected using a ZEISS Gemini SEM 500 microscope. Powder X-ray diffraction (XRD) measurements were performed using a diffractometer (Rigaku D/max 2500 PC) with Cu Kα radiation. Thermogravimetric analysis (TGA) was performed by using an STA449F3 NETZSCH scanning from 50 °C to 1000 °C, with a ramping rate of 10 °C min^{-1}. The photoluminescence spectra were measured using a Horiba iHR 550 spectrometer excited by an ultraviolet LED (peaked at 365 nm). The absorption spectra were captured using a Cary 5000 ultraviolet-visible-near infrared (UV-Vis-NIR) Agilent spectrometer with an integrating sphere.

First-principles calculations

First-principles calculations based on DFT are accomplished by using CASTEP.[29] The generalized-gradient-approximation (GGA) functional of the Perdew–Burke–Ernzerhof (PBE) type is employed here to calculate the electron–electron exchange–correlation. We selected ultrasoft pseudopotentials with a 350 eV cutoff energy for the plane wave basis set and a $2 \times 2 \times 2$ fine *k*-point mesh in the reciprocal space of Cs_2TiX_6 primitive cells. Crystal geometries and atom positions are optimized until the Hellmann–Feynman forces on the atoms are within 0.01 eV $Å^{-1}$ and the total energy convergence tolerance is set to 5×10^{-6} eV per atom.

Conflicts of interest

There are no conflicts to declare.

Acknowledgements

This work was supported by the National Natural Science Foundation of China (NSFC) 51601103 (L. Y.) and 1000 Youth Talents Program in China (L. Y.). X. S. also acknowledges State Key Laboratory of Advanced Optical Communication Systems and Networks (Shanghai Jiao Tong University, project 2018GZKF03005).

References

1 (*a*) H. J. Snaith, *Nat. Mater.*, 2018, **17**, 372; (*b*) Y.-H. Kim, H. Cho and T.-W. Lee, *Proc. Natl. Acad. Sci. U. S. A.*, 2016, **113**, 11694; (*c*) B. R. Sutherland and E. H. Sargent, *Nat. Photonics*, 2016, **10**, 295; (*d*) B. R. Sutherland and E. H. Sargent, *Nat. Photonics*, 2016, **10**, 295; (*e*) S. D. Stranks and H. J. Snaith, *Nat. Nanotechnol.*, 2015, **10**, 391.

2 (*a*) Y. Cao, N. Wang, H. Tian, J. Guo, Y. Wei, H. Chen, Y. Miao, W. Zou, K. Pan, Y. He, H. Cao, Y. Ke, M. Xu, Y. Wang, M. Yang, K. Du, Z. Fu, D. Kong, D. Dai, Y. Jin, G. Li, H. Li, Q. Peng, J. Wang and W. Huang, *Nature*, 2018, **562**, 249; (*b*) K. Lin, J. Xing, L. N. Quan, F. P. G. de Arquer, X. Gong, J. Lu, L. Xie, W. Zhao, D. Zhang, C. Yan, W. Li, X. Liu, Y. Lu, J. Kirman, E. H. Sargent, Q. Xiong and Z. Wei, *Nature*, 2018, **562**, 245.

3 (*a*) Q. Jiang, Y. Zhao, X. Zhang, X. Yang, Y. Chen, Z. Chu, Q. Ye, X. Li, Z. Yin and J. You, *Nat. Photonics*, 2019, **13**, 460; (*b*) T. Matsui, T. Yamamoto, T. Nishihara, R. Morisawa, T. Yokoyaya, T. Sekiguchi and T. Negami, *Adv. Mater.*, 2019, **31**, 1806823.

4 Z. Xiao, Z. Song and Y. Yan, *Adv. Mater.*, 2019, **31**, 1803792.

5 Q. Wei and Z. Ning, *Sci. China: Chem.*, 2019, **62**, 287.

6 D. Ju, X. Zheng, J. Yin, Z. Qiu, B. Türedi, X. Liu, Y. Dang, B. Cao, O. F. Mohammed, O. M. Bakr and X. Tao, *ACS Energy Lett.*, 2019, **4**, 228.

7 I. Kopacic, B. Friesenbichler, S. F. Hoefler, B. Kunert, H. Plank, T. Rath and G. Trimmel, *ACS Appl. Energy Mater.*, 2018, **1**, 343.

8 (*a*) Z. Wu, Q. Zhang, B. Li, Z. Shi, K. Xu, Y. Chen, Z. Ning and Q. Mi, *Chem. Mater.*, 2019, **31**, 4999; (*b*) L.-y. Huang and W. R. L. Lambrecht, *Phys. Rev. B: Condens. Matter Mater. Phys.*, 2013, **88**, 165203.

9 D. Cortecchia, H. A. Dewi, J. Yin, A. Bruno, S. Chen, T. Baikie, P. P. Boix, M. Grätzel, S. Mhaisalkar, C. Soci and N. Mathews, *Inorg. Chem.*, 2016, **55**, 1044.

10 M. Abulikemu, S. Ould-Chikh, X. Miao, E. Alarousu, B. Murali, G. O. Ngongang Ndjawa, J. Barbé, A. El Labban, A. Amassian and S. Del Gobbo, *J. Mater. Chem. A*, 2016, **4**, 12504.

11 B. Saparov, F. Hong, J.-P. Sun, H.-S. Duan, W. Meng, S. Cameron, I. G. Hill, Y. Yan and D. B. Mitzi, *Chem. Mater.*, 2015, **27**, 5622.

12 G. Volonakis, M. R. Filip, A. A. Haghighirad, N. Sakai, B. Wenger, H. J. Snaith and F. Giustino, *J. Phys. Chem. Lett.*, 2016, **7**, 1254.

13 M. Chen, M.-G. Ju, A. D. Carl, Y. Zong, R. L. Grimm, J. Gu, X. C. Zeng, Y. Zhou and N. P. Padture, *Joule*, 2018, **2**, 558.

14 M.-G. Ju, M. Chen, Y. Zhou, H. F. Garces, J. Dai, L. Ma, N. P. Padture and X. C. Zeng, *ACS Energy Lett.*, 2018, **3**, 297.

15 R. L. Lister and S. N. Flengas, *Can. J. Chem.*, 1963, **41**, 1548.

16 I. I. Kozhina and D. V. Korol'kov, *J. Struct. Chem.*, 1965, **6**, 84.
17 H. Cho, Y.-H. Kim, C. Wolf, H.-D. Lee and T.-W. Lee, *Adv. Mater.*, 2018, **30**, 1704587.
18 E. Meyer, D. Mutukwa, N. Zingwe and R. Taziwa, *Metals*, 2018, **8**, 667.
19 S. J. Zelewski, J. M. Urban, A. Surrente, D. K. Maude, A. Kuc, L. Schade, R. D. Johnson, M. Dollmann, P. K. Nayak, H. J. Snaith, P. Radaelli, R. Kudrawiec, R. J. Nicholas, P. Plochocka and M. Baranowski, *J. Mater. Chem. C*, 2019, **7**, 8350–8356.
20 H. Xiao, J. Tahir-Kheli and W. A. Goddard III, *J. Phys. Chem. Lett.*, 2011, **2**, 212.
21 J. Liu, X. Sun, D. Pan, X. Wang, L. C. Kimerling, T. L. Koch and J. Michel, *Opt. Express*, 2007, **15**, 11272.
22 (*a*) H. Huang, A. S. Susha, S. V. Kershaw, T. F. Hung and A. L. Rogach, *Adv. Sci.*, 2015, **2**, 1500194; (*b*) Z. Zhang, L. Shen, H. Zhang, L. Ding, G. Shao, X. Liang and W. Xiang, *Chem. Eng. J.*, 2019, **378**, 122125.
23 (*a*) J. Luo, X. Wang, S. Li, J. Liu, Y. Guo, G. Niu, L. Yao, Y. Fu, L. Gao, Q. Dong, C. Zhao, M. Leng, F. Ma, W. Liang, L. Wang, S. Jin, J. Han, L. Zhang, J. Etheridge, J. Wang, Y. Yan, E. H. Sargent and J. Tang, *Nature*, 2018, **563**, 541; (*b*) Y. Zhou, J. Chen, O. M. Bakr and H.-T. Sun, *Chem. Mater.*, 2018, **30**, 6589.
24 E. Mosconi, A. Amat, M. K. Nazeeruddin, M. Grätzel and F. De Angelis, *J. Phys. Chem. C*, 2013, **117**, 13902.
25 (*a*) X. Zheng, Y. Hou, H.-T. Sun, O. F. Mohammed, E. H. Sargent and O. M. Bakr, *J. Phys. Chem. Lett.*, 2019, **10**, 2629; (*b*) M. Abdi-Jalebi, Z. Andaji-Garmaroudi, S. Cacovich, C. Stavrakas, B. Philippe, J. M. Richter, M. Alsari, E. P. Booker, E. M. Hutter, A. J. Pearson, S. Lilliu, T. J. Savenije, H. Rensmo, G. Divitini, C. Ducati, R. H. Friend and S. D. Stranks, *Nature*, 2018, **555**, 497; (*c*) X. Yang, X. Zhang, J. Deng, Z. Chu, Q. Jiang, J. Meng, P. Wang, L. Zhang, Z. Yin and J. You, *Nat. Commun.*, 2018, **9**, 570; (*d*) P. Zhang, T. Zhang, Y. F. Wang, D. T. Liu, H. Xu, L. Chen, Y. B. Li, J. Wu, Z. D. Chen and S. Li, *J. Power Sources*, 2019, **439**, 9.
26 (*a*) F. Wang, T. Zhang, Y. F. Wang, D. Liu, P. Zhang, H. Chen, L. Ji, L. Chen, Z. D. Chen, J. Wu, X. Liu, Y. B. Li, Y. F. Wang and S. Li, *J. Mater. Chem. A*, 2019, **7**, 12166–12175; (*b*) D. T. Liu, H. L. Zheng, L. Ji, H. Chen, Y. F. Wang, P. Zhang, F. Wang, J. Wu, Z. Chen and S. Li, *J. Power Sources*, 2019, **441**, 227161.
27 (*a*) M. Ahmadi, T. Wu and B. Hu, *Adv. Mater.*, 2017, **29**, 1605242; (*b*) J. A. Steele, W. Pan, C. Martin, M. Keshavarz, E. Debroye, H. Yuan, S. Banerjee, E. Fron, D. Jonckheere, C. W. Kim, W. Baekelant, G. Niu, J. Tang, J. Vanacken, M. Van der Auweraer, J. Hofkens and M. B. J. Roeffaers, *Adv. Mater.*, 2018, **30**, 1870353; (*c*) Q. Jiang, M. Chen, J. Li, M. Wang, X. Zeng, T. Besara, J. Lu, Y. Xin, X. Shan, B. Pan, C. Wang, S. Lin, T. Siegrist, Q. Xiao and Z. Yu, *ACS Nano*, 2017, **11**, 1073.
28 (*a*) K. Saeki, Y. Wakai, Y. Fujimoto, M. Koshimizu, T. Yanagida, D. Nakauchi and K. Asai, *Jpn. J. Appl. Phys.*, 2016, **55**, 3; (*b*) K. Saeki, Y. Fujimoto, M. Koshimizu, D. Nakauchi, H. Tanaka, T. Yanagida and K. Asai, *Jpn. J. Appl. Phys.*, 2018, **57**, 4.
29 S. J. Clark, M. D. Segall, C. J. Pickard, P. J. Hasnip, M. I. Probert, K. Refson and M. C. Payne, *Z. Kristallogr. - Cryst. Mater.*, 2005, **220**, 567.